Experimental Thermal and Fluid Science 51 (2013) 183–188

Contents lists available at ScienceDirect

Experimental Thermal and Fluid Science

journal homepage: www.elsevier.com/locate/etfs

Experimental characterization of the effects of geometric parameters on evaporative pumping

Robert Crawford, Thomas E. Murphy, Alexandre K. da Silva *, Halil Berberoglu

Department of Mechanical Engineering, University of Texas at Austin, Austin, TX, United States

ARTICLE INFO

Article history:
Received 5 October 2012
Received in revised form 14 May 2013
Accepted 25 July 2013
Available online 1 August 2013

Keywords:
Evaporative pumping
Phase change
Porous membrane

ABSTRACT

This study is interested in determining the experimental relation between the suction pressure and evaporation rate from the upper surface of a flat, thin porous membrane, which naturally draws water from a reservoir, and its microchannel feeding system. The effects of three main design parameters of a water delivery system on the evaporation rate of the membrane are considered: (i) the diameter of the microchannels irrigating the membrane, (ii) the length of the irrigating microchannels, and (iii) the surface area of the membrane. Additionally, we also evaluated the effect of the pumping height (i.e., the vertical distance between the membrane and the main reservoir) on the evaporation rates for the three design parameters. While the maximum evaporation rate from the membrane is a function of the membrane's properties (e.g., permeability and porosity), as well as the ambient conditions (e.g., temperature, pressure and humidity), this study focused on determining the geometric parameters of closed water-feeding microchannels that properly hydrate a porous membrane while not impeding evaporation. Results indicated that the evaporation rate was mostly unaffected by the channel dimensions considered. Moreover, evaporation rates increased with increasing surface area (between 20.3 cm^2 and 176.7 cm^2) but at a decreasing rate of return. Finally, the suction pressures achieved were inversely related to hydrodynamic pressure drop and were unaffected by the membrane diameter.

1. Introduction

The ability to move small, accurate amounts of fluid, less than 1 ml per minute, has become increasingly in demand in a wide range of fields from medicine to electronics. In biological applications, precise dosing is required for medicine delivery [1]. In chemistry, species separation is desired for mass spectrometer analysis [2]. With the continual shrinking of electronics, small amounts of liquid are used in microelectronics cooling [3–5]. The applications go on and on for pumping small amounts of fluid including circulation, metering, and point to point transfer. Until recently, the prevailing method has been to use micropumps.

Micropumps have been offered in both a valve and valveless configuration [6]. For the most part, valve micropumps rely on electromechanic devices that utilize an oscillating motion to displace fluid, e.g. electromagnetic [7], electrostatic [8], piezoelectric [9], and thermopneumatic [10] actuation. However, the oscillation often produces pulsating streams, which can be undesirable for certain applications. Valveless micropumps provide continuous flow by directly imparting energy to the fluid. Many techniques have been developed in this area including electrochemical [11], electrohydro-dynamic [12], electrokinetic [13], electroosmotic [14], and magneto-hydrodynamic [15]. One of the main drawbacks of valveless pumps, however, is related to substantial power requirements [6].

In light of the limitations mentioned, a new branch has emerged in pump research based on transpiration. Transpiration is the continuous, passive flow of water in plants from the soil to the atmosphere. In plants, whose height is greater than the capability of capillary action to overcome gravity, transpiration is relied on for moving water and minerals throughout the body via xylem [16]. Additionally, transpiration prevents leaves from overheating in direct sunlight [17,18]. One of the main advantages of transpiration is that it is a passive evaporative pumping operation that does not require the assistance of pumps, valves or moving parts, making it a robust system with diminished maintenance requirements. Furthermore, the process is noiseless and does not cause vibrations, which could be extremely important in certain applications.

According to Dixon and Joly's Cohesion Theory, suction pressures up to −1.0 MPa can be imposed by root systems, pulling water from the soil to replenish what was evaporated from the leaves [19–21]; a good example being the redwood trees of the Pacific Northwest, which can be over 100 m high [22]. While more extensive investigations have shown that transpiration is actually more complicated and utilizes additional processes (e.g. evapora-

* Corresponding author. Tel.: +1 (512) 232 0866.
E-mail address: akds@mail.utexas.edu (A.K. da Silva).

0894-1777/$ - see front matter © 2013 Elsevier Inc. All rights reserved.
http://dx.doi.org/10.1016/j.expthermflusci.2013.07.013

tion, osmosis, wicking and others) than Cohesion Theory first proposed [23], Cohesion Theory is a good basis for this preliminary investigation.

Previous work has been done to mimic transpiration in plants. For example, Wheeler and Stroock [21] constructed a synthetic tree structure that used evaporation from a membrane to pull water through a microfluidic channel. Results indicated flow rates of 2.3 nl/s, representing a calculated pressure drop of 10 kPa. Borno et al. [24] also used microfabrication to build an evaporation driven synthetic leaf reaching measured flow velocities up to 1.5 cm/s. Moreover, several groups have used evaporation from porous media as a passive means to move liquid through microfluidic channels for biomedical applications [25–27]. In Guan et al. [25] setup, the experimental evaporative micropump provided a consistent flow rate of 46 nl/s for vertical displacements up to 2 m. In a later study, the same group investigated the effects of ambient relative humidity, temperature, and evaporative surface area on flow rate provided by the micropump [26]. Li et al. [27] designed an evaporative micropump consisting of plant stomata-shaped evaporation apertures. Lynn and Dandy [28] used evaporation from a meniscus to drive flow through a microchannel network. In doing so, they were able to maintain a constant flow rate for a period of time exceeding 1 h.

In this study, we designed, constructed, and tested a low-tech evaporative pumping system that does not require microfabrication. The system was designed such that we could mimic a leaf's evaporative surface, since this can be considered a two-dimensional ramifying structure [16]. The "xylem" of the microfluidic system was a combination of polyetheretherketone (PEEK) microchannels and Tygon tubing for larger passageways. The evaporative surface was a thin porous membrane (Fisherbrand Glass Fiber Filter Circles, G6). Three parameters were investigated: (i) the diameter of the channel feeding the membrane, (ii) the length of the microchannel, and (iii) surface area of the evaporative surface. Additionally, the suction pressure of evaporation was measured and related to pumping height of the system (i.e., the height difference between the evaporating surface and the supply reservoir). The aforementioned parameters have been parametrically investigated to determine when each limits the self-driven evaporation process.

2. Materials and methods

2.1. Experimental setup

The evaporative pumping system consisted of a porous membrane connected to a distilled water reservoir via a microchannel and tubing, as shown in Fig. 1. The reservoir sat on a balance (Denver Instruments PI – 214, range 0–210 g, resolution 0.1 mg) which recorded mass loss to a spreadsheet file using Denver Instruments' proprietary software. To prevent unwanted evaporative losses from the reservoir to the atmosphere, its top was covered with a lid while a 2 mm diameter pinhole maintained the reservoir pressure equal to the room pressure. Due to the slow rate of mass decrease in the reservoir, it was assumed that the interior of the reservoir was at the same pressure as the air in the room. Because all mass loss from the water reservoir was due to evaporation from the porous membrane, the balance was effectively recording the evaporation rate from the membrane. Due to the balance's sensitivity to air currents, this was placed in a specially designed acrylic isolation box so the balance sliding door could remain open during testing. Additionally, the mass loss from the covered reservoir by itself was confirmed to be negligible when the balance was left to record mass while no membrane evaporation was occurring. The mass rate decrease was found to be less than 1% of the lowest evaporation rate that would be tested as a result of the experimental setup configurations.

The microchannels used to irrigate the membrane were high-pressure polyetheretherketone (PEEK) tubing, which fit snuggly into a small perpendicular hole in the center of an acrylic plate surface that served as support for the membrane. Sealant was applied to the underside of the acrylic where the tube entered to prevent leakage. Three values of channel diameter, length, and membrane area could be interchanged: (i) diameters of 127, 177.8, and 254 μm, (ii) lengths of 2.54, 7.62, and 15.24 cm, and (iii) areas of 20.3, 81.1 and 176.7 cm^2 (before wetting). Additional tubing, 1/8th inch ID Tygon tubing, was used to connect the microchannel to the reservoir – a color scheme[1] was used in Fig. 1 in order to identify the PEEK channels and the Tygon tubing, red and grey tubing, respectively. All tubing was purged of air bubbles to ensure single phase flow. The system also featured Swagelok valves for turning the system on and off – the operation procedure will be discussed later. A parallel study showed that any pressure drop in the Tygon tubing and connectors was negligible compared to the pressure drop in the microchannel and did not affect the system. Additionally, the Tygon tubing produced negligible capillary rise of the fluid.

Two additional lines were teed off from the main supply line. One line connected to a ±34.475 kPa differential pressure sensor (Omega PX26-005DV, calibrated uncertainty was 0.017 kPa at 95% confidence) with one side open to atmosphere. Pressure was calculated using the density of water at atmospheric pressure and a temperature of 23.5 °C. The other line connected to another reservoir placed high above the channel. The purpose of this second reservoir was for initially wetting the membrane to start the system. It too featured an on/off valve.

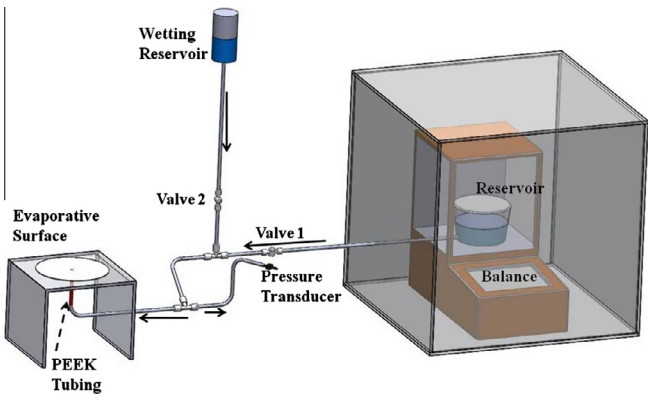

Fig. 1. Experimental evaporative pumping system setup.

2.2. Membrane characterization

The evaporative surface was a thin porous membrane (Fisherbrand Glass Fiber Filter Circles G6). The microstructure was examined using a Jeol JSM-5610 scanning electron microscope (SEM). The structure was of a random nature with much interlocking between fibers as shown in Fig. 2a–c. The fibers were relatively smooth, constant diameter rods ranging in diameter up to ~3 μm; however, the fiber length could not be identified. Spacing between fibers was estimated to be up to 7 μm. The size of the fibers and spacing between fibers plays a major role in the capillary spreading of a fluid in the membrane.

[1] For interpretation of color in Fig. 1, the reader is referred to the web version of this article.

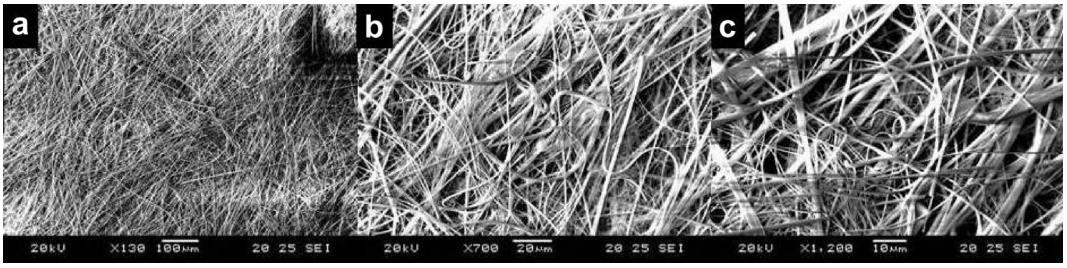

Fig. 2. SEM images showing the structure of the porous membrane evaporative surface.

2.3. Experimental procedure

To begin the experiment, the desired channel diameter and length and membrane area were selected. A dry membrane was placed on the acrylic sheet and centered on the outlet of the channel. The height of the reservoir's free surface was brought to the height of the membrane. Valve 1 (see Fig. 1) was closed and valve 2 was opened to begin the "forced" wetting process of the membrane. The aid of gravity was used in the initial wetting of the membrane because this study investigated the steady state flow rather than the initial wetting phenomena. Once the entire membrane was visually confirmed to be wet, valve 2 was closed and valve 1 was immediately opened to begin the evaporative pumping process. The balance recorded measurements of the mass loss from the reservoir every minute to a spreadsheet file. In the event that the membrane was initially overwatered, the system would self-regulate, i.e. wait until excess water had evaporated from the membrane before drawing replenishment from the reservoir. Conversely, if the membrane was initially under watered, an initial period of high evaporation rates were measured until the membrane reached its steady state wetness. Temperature and humidity of the room were recorded using a Fisher Scientific Fisherbrand traceable Hygrometer/Thermometer. While these two factors were not controlled during the tests, over the course of all experiments, the temperature of the room remained at 23.5 ± 0.5 °C while the humidity was 50% ± 5%. During any particular trial, however, because of the short duration of a test, the temperature and humidity remained relatively constant within 0.2 °C and 3% humidity. It is important to note that humidity is indeed a relevant factor when determining evaporation rates; however, this preliminary study only focused on the parametric effect of the three variables previously discussed.

Steady state operation of the system was determined by a constant evaporation rate (within 5%) for at least 30 min. Upon reaching steady state, the reservoir was disconnected by closing valve 1. This left the evaporative surface only in contact with the pressure transducer. Over the course of up to two hours following the closing of valve 1, increasingly negative pressures were recorded as the evaporative surface dried out. The experiment was considered finished when the suction pressure returned to roughly a zero pressure differential, which corresponded to the column of water breaking from the membrane.

For illustration purposes, the propagation of water in a membrane can be seen in Fig. 3 showing the movement of the water from its point source in the center, outward. The propagation of the fluid was generally even and smooth. This visualization was performed by placing a drop of blue food dye at the point source during steady state system operation – it can be seen that the dye was being pushed/pulled away from the center of the membrane as time elapsed. Also, it was found that food dye used for visualization did not affect the evaporation rate, even though it was just used on Fig. 3 to qualitatively show the water flow through the membrane.

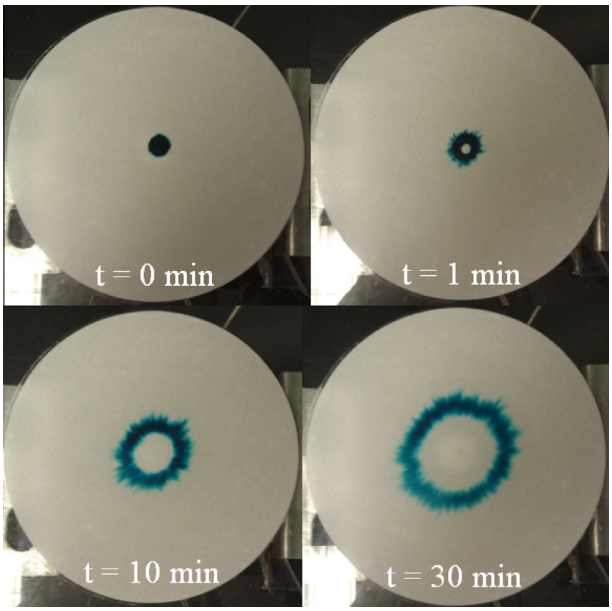

Fig. 3. Propagation of fluid in the porous membrane from the microchannel point source.

A minimum of three experiments were performed under the same conditions. A new membrane was used for each test. It was found that rewetted membranes (membranes that were tested, dried out and then wetted again) produced evaporate rates that were lower than new membranes. This may be a property specific to this membrane and may be different for other membranes; however, since membrane degradation it was not a focus of this investigation, this factor was eliminated for the investigation.

3. Results and discussion

The results of the parametric study to determine the effect of specific parameters on evaporative pumping, namely (i) microchannel diameter, (ii) length of the microchannel and (iii) evaporative surface membrane diameter, are presented next. Representative results are shown in Fig. 4 for steady state conditions of channels 254 µm in diameter and 2.54 cm in length with evaporative surface membrane diameters of 5.08, 10.16, and 15 cm. Between trials, the results were repeatable with an evaporation rate of approximately 3.7, 12.3, and 22.3 mg/min, respectively. Slight variations in evaporation rates, within 5% of the average evaporation rates across all trials, were attributed to the variations between test pieces. For instance, obtaining a smooth cut of the PEEK tubing was difficult. Thus, each tubing and test piece had its own unique surface imperfections, possibly affecting the contact between the evaporative membrane and the tubing.

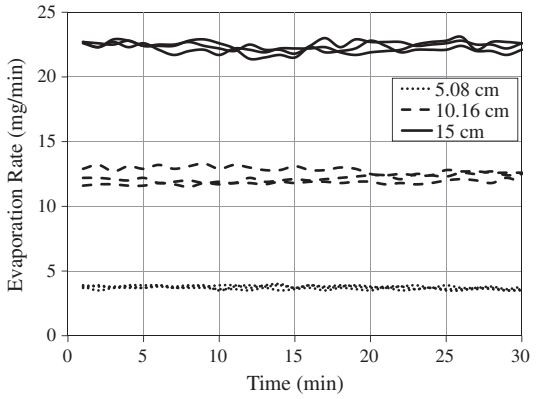

Fig. 4. Typical data collection of mass evaporation rate showing repeatability between trials. Parameters: 254 μm channel diameter, 2.54 cm channel length, and surface diameters of 5.08, 10.16, and 15 cm.

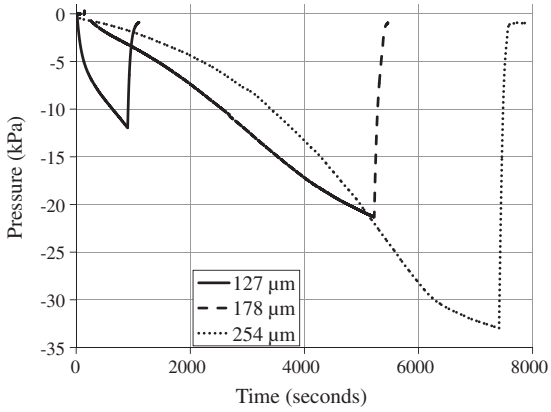

Fig. 5. Typical suction pressures as the membrane dries out for varying microchannel diameters. Parameters: channel length of 2.54 cm and membrane diameter of 15 cm.

Additionally, the suction capability of the evaporative membrane was also measured as a function of the tubing diameter. Typical trials are presented in Fig. 5 for all three microchannels tested (i.e., diameters of 127, 177.8, and 254 μm) at a length of 2.54 cm and a membrane diameter of 15 cm. While the results show that there was no significant effect on the evaporation rate other than what was stated earlier regarding the variations in test pieces, increasing the tube diameter did increase the maximum suction pressure attainable. Also, it can be observed for all cases that the suction pressure immediately began increasing when the membrane was disconnected from the water reservoir, and that the suction rate increased as the tubing diameter decreased. Furthermore, Fig. 5 shows that all tests experienced a period of constant suction rate increase followed by a sharp increase in pressure. As membrane dry out occurred, evaporation generated a tensile stress in the rigid space that was the membrane/water column assembly, which was registered by the pressure transducer. The suction pressure increased until it reached a pressure at which time, the seal between the membrane and tubing broke, causing air to rush in, returning the water in the tubing to atmospheric pressure. The seal breakage pressure can be estimated using the Laplace–Young equation, $P_c = 2\gamma\cos\theta/r$, where γ is the surface tension, θ is the contact angle of water and r is the radius of the pore [29,30]. For the pore radius of the membrane, 4 μm, the capillary pressure was roughly 35 kPa, which matched, in a magnitude sense, the maximum pressure reached for the tubing with the lowest pressure drop. One possible explanation for the effect of the tubing diameter on the suction rate and the maximum suction pressure had to do with the fact that, as the tubing diameter decreased, it had to overcome larger hydrodynamic forces. This led to the thought that if the evaporative surface was raised above the reservoir, larger diameter tubing would allow for greater height differences with smaller performance impacts when passive pumping was employed. Finally, it was also interesting to realize that one can determine pumping heights, by simply dividing the suction pressure by gravity and the density of the fluid. For example, with a suction pressure of −30 kPa, which was close to the maximum suction pressure for the tubing with a diameter of 254 μm, the system should pump to roughly 3.0 m.

The next parameter to be investigated was the tube length. Tests were performed using tubing of varying lengths with diameters of 254 μm and evaporative membrane diameters of 15 cm. Again, the tube length did not affect the evaporation rate for the dimensions tested. However, its effect was observable in the suction pressure that could be obtained, as shown in Fig. 6. Larger suction pressures were reached with shorter lengths, possibly for the same hydrodynamic reasoning as why channel diameter affected pressure. At increasing lengths, the height difference between evaporative surface and the reservoir would detrimentally impact the system's performance. Also, it is expected that at some length, the system would not be able to overcome the pressure drop in the tubing and pumping would cease.

Lastly for dimensional parameters, the evaporative surface diameter was varied. While the measured data is not shown, the suction pressure remained unaffected with varying surface diameter (areas). This suggested that the suction pressure was governed mostly by the microchannel parameters and microchannel/membrane connection. On the other hand, the evaporation rate increased with evaporative surface area, as shown in Fig. 7. As expected, the relationship was nonlinear with increases in surface diameter yielding diminishing increases in evaporation rate (left y-axis). This was more obvious when the average evaporation rate was normalized per unit of surface area (right y-axis). Increasing surface areas led to lower evaporation rates per unit area. That was because not enough fluid was present to saturate the outer regions due to evaporative losses. In a system fed by a point source, like the one discussed in this paper, fluid transported in the radial direction would be completely evaporated at a certain radius. For this system, following the trend of the normalized evaporation rate, it was estimated that the critical radius was roughly 20 cm, as the membrane material at a radius greater than this critical radius would most likely not receive fluid. It is expected that the interface between wetted and non-wetted areas within a membrane would move depending on membrane properties such as permeability, porosity, and fiber spacing.

Even though temperature was not the focus of this paper, the temperature profile for a 15 cm evaporating membrane at steady

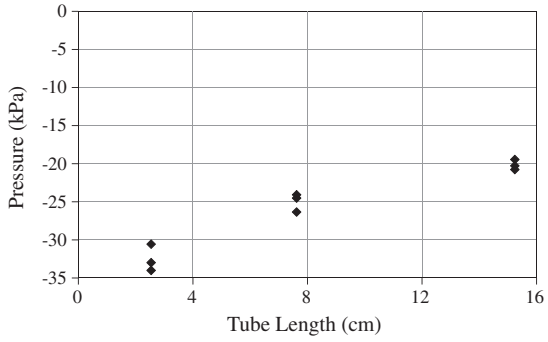

Fig. 6. Effect of the microchannel length on the suction pressure. Parameters: 254 μm channel diameter, 15 cm membrane diameter.

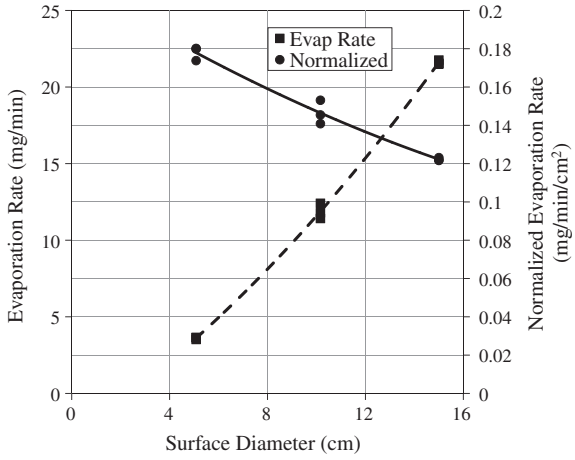

Fig. 7. Effect of the membrane diameter on the absolute and normalized evaporation rates. Parameters: 254 μm channel diameter, 2.54 cm channel length.

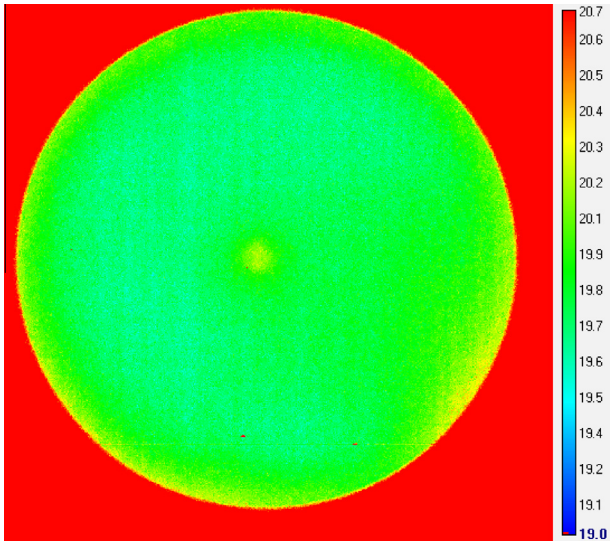

Fig. 8. IR imaging showing the temperature profile (°C) of a 15 cm membrane at steady state operation.

state operation was captured with an IR camera (FLIR A615, 2% accuracy), Fig. 8. In order to calibrate the camera, the emissivity, ε, was needed of a wet membrane. A spectrophotometer (Optronics Laboratories, OL-750) was used to measure the reflectivity, ρ, of a wet membrane backed by acrylic over the wavelength of 350 to 2500 nm. With Kirchhoff's Law stating that the emissivity is equal to the absorptivity, α, considering no transmission, the emissivity was measured to be around ~0.45. The IR camera's readings were confirmed by viewing a copper plate of known emissivity and comparing against an imbedded thermocouple. As shown in Fig. 8, minor temperature variations can be seen across the membrane ranging from 19.6 to 20.2 °C; recall that the room temperature was 23.5 ± 0.5 °C. The highest temperature can be seen at the point source where the membrane met the PEEK tubing and water was being supplied. This is most likely due to the temperature of the reservoir fluid being at room temperature before reaching the membrane. Moving radial outward, the majority of the membrane was 19.6–19.8 °C. Approaching the edge of this membrane diameter, it can be seen that the temperature began to increase. Recall that the localized evaporation rate would have been lower, further away from the point source based on the normalized evaporation rate analysis. It is anticipated that the temperature in the membrane, moving in the radial direction, would increase until reaching room temperature after the critical radius threshold had been reached as discussed in the normalized evaporation analysis.

4. Conclusions

In this paper, a preliminary parametric analysis was performed to identify the limiting physical aspects of an evaporative pumping system. Three components of a system were investigated, namely (i) microchannel diameter, (ii) length of the microchannel and (iii) diameter of the evaporative porous membrane. Distilled water was evaporated from the surface of a thin porous membrane connected to a reservoir via a PEEK microchannel. The reservoir sat on a balance that measured mass loss out of the reservoir by evaporation from the membrane. Additionally, the suction pressure was measured when the saturated membrane was disengaged from the reservoir.

The results indicated that at the channel dimensions tested, evaporation rate did not vary. Channel dimensions did, however, affect the suction pressure. Maximum suction pressures were obtained from channels of larger diameters and shorter lengths. Larger suction pressures would allow for greater height disparities between the evaporative membrane and the free surface of the reservoir while minimizing the impact on the passively pumping system. Greater surface areas, however, allowed for larger evaporation rates with a decreasing rate of return on the evaporation rate gained but did not affect the suction pressure.

Acknowledgements

The authors acknowledge the support of the National Science Foundation (NSF) Integrative Graduate Education and Research Traineeship (IGERT) program (Grant Number: 0966298). We would like to acknowledge Mr. Albert Phan from The University of Texas at Austin for his help on the microstructure imaging and preparation of graphics.

References

[1] D.J. Laser, J.G. Santiago, A review of micropumps, J. Micromech. Microeng. 14 (2004) R35–R64, http://dx.doi.org/10.1088/0960-1317/14/6/R01.
[2] P.A. Limbach, Z. Meng, Integrating micromachined devices with modern mass spectrometry, The Analyst 127 (2002) 693–700, http://dx.doi.org/10.1039/b200143h.
[3] D.B. Tuckerman, R.F.W. Pease, High-performance heat sinking for VLSI, IEEE Electron. Dev. Lett. EDL-2 (1981) 126–129.
[4] L. Jiang, J. Mikkelsen, J.-Mo Koo, Closed-loop electroosmotic microchannel cooling system for VLSI circuits, IEEE Trans. Compon. Packag. Technol. 25 (2002) 347–355.
[5] L. Zhang, J.-Mo Koo, L. Jiang, Measurements and modeling of two-phase flow in microchannels with nearly constant heat flux boundary conditions, J. Microelectromech. Syst. 11 (2002) 12–19.
[6] X. Du, T.S. Zhao, J. Luo, Continuous microliquid delivery by evaporation on a gradient-capillary microstructure surface, J. Micromech. Microeng. 21 (2011) 095004, http://dx.doi.org/10.1088/0960-1317/21/9/095004.
[7] S. Bohm, W. Olthuis, P. Bergveld, A plastic micropump constructed with conventional techniques and materials, Sens. Actuat. A: Phys. 77 (1999) 223–228.
[8] R. Zengerle, A. Richter, H. Sandmaier, A micromembrane pump with electrostatic actuation, Micro Electro Mech. Syst. (1992) 19–24.
[9] M. Carrozza, N. Croce, B. Magnani, P. Dario, A piezoelectric-driven stereolithography-fabricated micropump, J. Micromech. Micromech. 5 (1995) 177–179.
[10] F.C.M. Van De Pol, D. Wonnink, M. Elwenspoek, A thermo-pneumatic actuation principle for a microminiature pump and other micromechanical devices, Sens. Actuat. 17 (1989) 139–143.
[11] D. O'Keefe, C. O'Herlihy, Y. Gross, J. Kelly, Patient-controlled analgesia using a miniature electrochemically driven infusion pump, Br. J. Anaesthesia. 73 (1994) 843–846.
[12] A. Richter, A. Plettner, K. Hofmann, Electrohydrodynamic pumping and flow measurement, Micro Electro Mech. Syst., MEMS Proc. Invest. Micro Struct., Sens., Actuat., Mach. Robots IEEE (1991) 271–276.

[13] A. Manz, C. Effenhauser, N. Burggraf, Electroosmotic pumping and electrophoretic separations for miniaturized chemical analysis systems, J. Micromech Microeng. 4 (1994) 257–265.
[14] A. Olsson, P. Enoksson, G. Stemme, E. Stemme, Micromachined flat-walled, J. Microelectromech. Syst. 6 (1997) 161–166.
[15] J. Jang, S. Lee, Theoretical and experimental study of MHD (magnetohydrodynamic) micropump, Sens. Actuat. A: Phys. 80 (2000) 84–89.
[16] A. Roth-Nebelsick, D. Uhl, V. Mosbrugger, H. Kerp, Evolution and Function of Leaf Venation Architecture: A Review, Ann. Bot. 87 (2001) 553–566, http://dx.doi.org/10.1006/anbo.2001.1391.
[17] O.L. Lange, Untersuchungen über Wärmehaushalt und Hitzeresistenz mauretanischer Wüsten- und Savannenpflanzen, Flora 147 (1959) 595–651.
[18] O.L. Lange, Die Photosynthese der Flechten bei tiefen Temperaturen und nach Frostperioden, Ber. Dt. Bot. Ges. 75 (1963) 351–352.
[19] H. Dixon, J. Joly, On the ascent of sap, Philos. Trans. R. Soc. London 186 (1895) 563–576.
[20] M. Zwieniecki, P.J. Melcher, C.K. Boyce, et al., Hydraulic architecture of leaf venation in *Laurus nobilis* L, Plant, Cell Environ. 25 (2002) 1445–1450, http://dx.doi.org/10.1046/j.1365-3040.2002.00922.x.
[21] T.D. Wheeler, A.D. Stroock, The transpiration of water at negative pressures in a synthetic tree, Nature 455 (2008) 208–212, http://dx.doi.org/10.1038/nature07226.
[22] N. Goedecke, J. Eijkel, A. Manz, Evaporation driven pumping for chromatography application, Lab On a Chip 2 (2002) 219–223, http://dx.doi.org/10.1039/b208031c.
[23] U. Zimmermann, F. Meinzer, F. Bentrup, How does water ascend in tall trees and other vascular plants?, Ann Bot. 76 (1995) 545–551.
[24] R.T. Borno, J.D. Steinmeyer, M.M. Maharbiz, Charge-pumping in a synthetic leaf for harvesting energy from evaporation-driven flows, Appl. Phys. Lett. 95 (2009) 013705-1–013705-3, http://dx.doi.org/10.1063/1.3157144.
[25] Y.-X. Guan, Z.-R. Xu, J. Dai, Z.-L. Fang, The use of a micropump based on capillary and evaporation effects in a microfluidic flow injection chemiluminescence system, Talanta 68 (2006) 1384–1389, http://dx.doi.org/10.1016/j.talanta.2005.08.021.
[26] Z. Xu, C. Zhong, Y. Guan, X. Chen, J. Wang, Z.L. Fang, A microfluidic flow injection system for DNA assay with fluids driven by an on-chip integrated pump based on capillary and evaporation effects, Lab On a Chip 8 (10) (2008) 1658–1663, http://dx.doi.org/10.1039/b805774e.
[27] J.-min Li, C. Liu, Z. Xu, et al., A bio-inspired micropump based on stomatal transpiration in plants, Lab On a Chip 11 (2011) 2785–2789, http://dx.doi.org/10.1039/c1lc20313d.
[28] N.S. Lynn, D. Dandy, Passive microfluidic pumping using coupled capillary/evaporation effects, Lab On a Chip 9 (2009) 3422–3429, http://dx.doi.org/10.1039/b912213c.
[29] K.J. Lee, J.H. Nam, C.J. Kim, Pore-network analysis of two-phase water transport in gas diffusion layers of polymer electrolyte membrane fuel cells, Electrochimica Acta 54 (2009) 1166–1176.
[30] G.M.G. Teige, C. Hermanrud, H.G. Rueslatten, Membrane seal leakage in non-fractured caprocks by the formation of oil-wet flow paths, J. Pet. Geol. 34 (1) (2011) 45–52.